高等学校化学学报
CHEMICAL JOURNAL OF CHINESE UNIVERSITIES
研究论文

具有聚集诱导发光性质的高灵敏度和高光稳定性的脂滴荧光探针

高　鑫[1#], 卿　佳[1#], 胡祎辰[2,3#], 上官之春[4], 梁同玲[2],
周永胜[1], 张关心[2], 张德清[2,3]

(1. 北京大学口腔医学院口腔修复科, 国家口腔医学中心, 口腔疾病国家临床医学研究中心, 口腔生物材料与数字诊疗设备国家工程研究中心, 颅颌面组织生物智造与修复再生北京市重点实验室, 国家卫生健康委员会数字口腔医学重点实验室, 国家药品监督管理局口腔材料重点实验室, 北京 100081;
2. 中国科学院化学研究所分子科学国家研究中心, 中国科学院有机固体重点实验室, 北京 100190;
3. 中国科学院大学化学科学学院, 北京 100190;
4. 温州大学化学与材料工程学院, 温州生物健康材料与化学重点实验室, 温州 325027)

摘要　设计合成了2种新型聚集诱导发光(AIE)探针TPA-H与TPA-2F. 这2种探针均表现出优异的生物相容性(浓度高达50 μmol/L时, 细胞存活率仍超过90%)和脂滴靶向特异性. 在3T3-L1脂肪细胞的早期分化过程中, TPA-2F与TPA-H均能清晰显像BODIPY难以检测的微小以及新生脂滴, 显示出更优的成像灵敏度. 此外, TPA-2F展现出高的光稳定性, 在连续100次激光扫描后, 其荧光强度仍保持初始值的90%以上. 研究结果不仅提供了2种高性能的脂滴成像工具, 更凸显了AIE发光材料在细胞器特异性生物成像中的应用潜力, 为脂质相关代谢疾病的早期诊断与机制研究提供了新的可能途径.

关键词　聚集诱导发光(AIE); 荧光成像; 脂滴; 光稳定性

中图分类号　O657　　**文献标志码**　A　　doi: 10.7503/cjcu20250410

Novel AIE Fluorescent Probes for Ultrahigh Sensitivity and High Photostability in Lipid Droplets Imaging

GAO Xin[1#], QING Jia[1#], HU Yichen[2,3#], SHANGGUAN Zhichun[4], LIANG Tongling[2], ZHOU Yongsheng[1*], ZHANG Guanxin[2*], ZHANG Deqing[2,3]

(*1. Department of Prosthodontics, Peking University School and Hospital of Stomatology & National Center for Stomatology & National Clinical Research Center for Oral Diseases & National Engineering Research Center of Oral Biomaterials and Digital Medical Devices & Beijing Key Laboratory of Digital Stomatology & NHC Key Laboratory of Digital Stomatology & NMPA Key Laboratory for Dental Materials, Beijing* 100081, *China*;
2. Beijing National Laboratory for Molecular Sciences, CAS Key Laboratory of Organic Solids, Institute of Chemistry, Chinese Academy of Sciences, Beijing 100190, *China*;
3. School of Chemical Sciences, University of Chinese Academy of Sciences, Beijing 100190, *China*;
4. College of Chemistry and Materials Engineering, Wenzhou University, Key Lab of Biohealth Materials and Chemistry of Wenzhou, Wenzhou 325027, *China*)

收稿日期: 2025-12-29. 网络首发日期: 2026-01-15.

联系人简介: 张关心, 男, 博士, 研究员, 主要从事有机光电材料方面的研究. E-mail: gxzhang@iccas.ac.cn
周永胜, 男, 博士, 教授, 主要从事口腔颌面组织缺损的生物再生性修复和数字化智能化仿生替代性修复与治疗方面的研究. E-mail: kqzhouysh@hsc.pku.edu.cn

基金项目: 国家自然科学基金(批准号: 82530030, 82270954, 22021002)资助.
Supported by the National Natural Science Foundation of China(Nos. 82530030, 82270954, 22021002).

共同第一作者.

Abstract Two novel aggregation-induced emission (AIE)-active probes, TPA-H and TPA-2F, were designed and synthesized based on a triphenylamine (TPA) core. Systematic characterization demonstrated that both probes exhibit excellent biocompatibility (cell viability>90% at concentrations up to 50 μmol/L) and outstanding LD-targeting specificity with minimal colocalization with other organelles such as mitochondria and lysosomes. During early differentiation of 3T3-L1 adipocytes, both TPA-2F and TPA-H clearly visualized small and nascent LDs that were difficult to be detected with BODIPY, indicating superior imaging sensitivity compared to the existing fluorescent probes for LDs. Moreover, TPA-2F demonstrated exceptional photostability, retaining over 90% of its initial fluorescence intensity after 100 continuous laser scanning cycles, significantly outperforming TPA-H. This work not only provides two high-performance LD imaging tools but also highlights the potential of AIE luminogens (AIEgens) in organelle-specific bioimaging, offering promising avenues for early diagnosis and mechanistic research of lipid-related metabolic diseases.

Keywords Aggregation-induced emission (AIE); Fluorescence imaging; Lipid Droplets; Photostability

1 Introduction

Lipid droplets (LDs), once considered inert intracellular lipid storage depots, are now recognized as dynamic organelles central to cellular energy metabolism, membrane biosynthesis, and signaling[1—3]. Their dysregulation is closely implicated in metabolic disorders such as obesity, fatty liver disease, and diabetes[4—6]. Consequently, precise visualization of LD dynamics —— particularly their biogenesis, growth, and interaction —— has become a critical objective in both basic cell biology and clinical research[7—9]. Fluorescence microscopy serves as a primary tool for this purpose, with commercial dyes like BODIPY 493/503 being widely adopted. However, these conventional probes often suffer from limitations such as aggregation-caused quenching (ACQ), which reduces their brightness in the densely packed LD core, and insufficient photostability, hindering long-term tracking[10—12]. Crucially, their sensitivity in detecting small, nascent LDs during early formation stages remains inadequate (Table S1, see the Supporting Information of this paper), leaving a significant gap in our ability to monitor the initial phases of lipid accumulation, a key event in the pathogenesis of metabolic diseases[13—15].

Aggregation-induced emission luminogens (AIEgens) have emerged as a promising alternative to address these challenges[16—21]. Compared to ACQ fluorophores, AIEgens exhibit enhanced fluorescence in the aggregated state, making them particularly suitable for imaging within the hydrophobic environment of lipid droplets (LDs)[22—24]. Triphenylamine (TPA) has been identified in previous studies as an effective moiety for targeting LDs[25—29]. For instance, Tang and co-workers developed a red-emissive AIE probe featuring a triphenylamine donor and a 2-benzothiazoleacetonitrile acceptor, which specifically stains LDs and enables visualization of their polarity distribution in live cells and tissues[29]. However, most existing TPA-based AIE probes are excited at wavelengths below 500 nm, limiting their applicability for *in vivo* studies.

Herein, we report two triphenylamine-based molecules, TPA-2F and TPA-H, functionalized with a strong electron-accepting unit——either 2-(3-oxo-2,3-dihydroinden-1-ylidene) malononitrile or 2-(5,6-difluoro-3-oxo-2,3-dihydro-1H-inden-1-ylidene) malononitrile. The incorporation of these strong acceptors is expected to redshift their absorption and emission bands to the NIR region. The results show that both compounds exhibit aggregation-induced emission (AIE), with absorption maxima near 600 nm and emission maxima longer than 700 nm. Moreover, these two compounds exhibit excellent specificity toward lipid droplets (LDs), showing minimal off-target localization in other organelles such as mitochondria and lysosomes. Notably, the introduction of fluorine atoms in TPA-2F endows it with enhanced resistance to photobleaching[30]. In cellular imaging, both TPA-2F and TPA-H outperformed the commercial dye BODIPY 493/503, particularly in visualizing small and

nascent LDs during the early stages of 3T3-L1 adipocyte differentiation. This heightened sensitivity enables the detection of initial lipid accumulation events that are otherwise difficult to observe. From a clinical perspective, the ability to monitor the formation of LD at an early stage enables these fluorescent probes to be a useful tool for studying the incipient phase of pathological lipid storage, which underlies conditions such as steatosis. Thus, these probes not only offer advanced imaging solutions for fundamental cell biology but also hold significant potential to facilitate early diagnosis and mechanistic investigation of lipid-associated metabolic disorders.

2 Experimental

2.1 Materials and Measurements

3-(Dicyanomethylidene) indan-1-one, 2-(5,6-difluoro-3-oxo-2,3-dihydro-1*H*-inden-1-ylidene) malononitrile were purchased from Energy Chemical(Shanghai, China). 4-[Bis(4-methoxyphenyl) amino] benzaldehyde was from Bide Pharmatech. Ltd. (Shanghai, China). The reagents and starting materials were commercially available and used without any further purification unless otherwise specified.

NMR spectra were recorded on Bruker AVANCE III 400 MHz spectrometers using tetramethylsilane (TMS) as internal reference. MALDI-FTICR-MS weas measured with a Bruker Solarix-XR high-resolution mass spectrometer. Absorption spectra were recorded on the Hitachi UH4150 spectrophotometer. Emission spectra were recorded on the Hitachi FP-6000 spectrometer. The diffraction data for the single crystals were collected with a Rigaku Saturn diffractometer with a CCD area detector.

2.2 Synthesis and Characterization

2.2.1 General synthetic procedure for TPA-H and TPA-2F To a solution of 1.0 mmol of 4-[bis(4-methoxyphenyl) amino] benzaldehyde in 10 mL of dry ethanol was added 3-(dicyanomethylene) indolin-2-one derivatives(1.0 mmol). The mixture was heated under reflux with stirring for 1 h. After cooling to room temperature, the resulting precipitate was collected by filtration, washed with ethanol, and recrystallized from ethanol to afford TPA-H and TPA-2F.

2.2.2 Synthesis of TPA-H By following the above general procedure and using 3-(dicyanomethylidene) indan-1-one as the reagent, TPA-H was obtained in a 92.5% yield. ^{1}H NMR(400 MHz, chloroform-*d*), δ: 8.66—8.64(m, 1H), 8.45(s, 1H), 8.20(d, *J*=8.7 Hz, 2H), 7.87—7.85(m, 1H), 7.75—7.67(m, 2H), 7.16(d, *J*=8.4 Hz, 4H), 6.94—6.83(m, 6H), 3.84(s, 6H). ^{13}C NMR(101 MHz, chloroform-*d*), δ: 187.08, 163.15, 158.00, 147.55, 139.69, 138.13, 137.39, 134.66, 134.12, 128.21, 124.87, 124.17, 123.66, 116.56, 115.19, 115.14, 114.93, 68.46, 55.56. HR-MS(MALDI, positive): *m/z* calcd. for $C_{33}H_{23}N_3O_3$ [M]$^+$: 509.1734, found: 509.1732.

2.2.3 Synthesis of TPA-2F By following the above general procedure and using 2-(5,6-difluoro-3-oxo-2,3-dihydro-1H-inden-1-ylidene) malononitrile as the reagent, TPA-2F was obtained in a 94.1% yield. ^{1}H NMR (400 MHz, chloroform-*d*), δ: 8.51—8.47(m, 1H), 8.42(s, 1H), 8.20—8.16(m, 2H), 7.61(t, *J*=7.7 Hz, 1H), 7.19—7.15(m, 4H), 6.95—6.91(m, 4H), 6.83(d, *J*=8.9 Hz, 2H), 3.84(s, 6H). ^{13}C NMR (101 MHz, chloroform-*d*), δ: 184.77, 160.93, 158.15, 154.79, 153.02, 147.74, 138.58, 137.57, 136.21, 136.13, 136.09, 134.94, 128.23, 123.98, 122.84, 116.50, 115.22, 114.80, 114.59, 114.53, 114.38, 112.62, 112.44, 68.66, 55.58. HR-MS (MALDI, positive): *m/z* calcd. for $C_{33}H_{21}F_2N_3O_3$ [M]$^+$: 545.1545, found: 545.1548.

2.3 3T3-L1 Cells Adipogenesis and Imaging

The 3T3-L1 preadipocytes were plated in DMEM(Gibco), which was supplemented with 10% bovine calf serum(Gibco). Two days following the attainment of confluence, the differentiation process was initiated by replacing the medium with DMEM supplemented with 10% FBS and the adipogenic cocktail, which consisted

of 0.5 mmol/L IBMX(MedChemExpress), 1.0 μmol/L dexamethasone(Alfa Aesar™), and 10 μg/mL insulin (MedChemExpress). Following a three-day incubation period, the differentiation medium was replaced with DMEM containing 10% FBS and 10 μg/mL insulin for a further two days. The cells should then be maintained in DMEM supplemented with 10% FBS, with the medium changed every two days.

A total of approximately 1.0×10^6 induced cells were seeded into a confocal dish and incubated for a period of 24 h. The cells were initially stained with BODIPY 493/505(Beyotime, C2053) in accordance with the instructions provided for a period of 20 min. After three PBS washes, the medium was refreshed and the cells were separately incubated for 30 min with 10 μmol/L TPA-2F or 10 μmol/L TPA-H. After washing, the cells were observed under an Olympus FV3000 confocal laser scanning microscope, with images captured using 570 nm excitation and 650—750 nm emission. The fluorescence intensity was subsequently analyzed using Image J.

The photostability of probes TPA-2F and TPA-H was evaluated by continuous laser scanning. After incubating cells with 10 μmol/L of each probe for 30 min, sequential imaging was performed on an Olympus FV3000 confocal microscope. Cells were subjected to 200 cycles of scanning with the excitation wavelength of 570 nm, and the interval time between cycles was 10 s; thus, the total acquisition time was 2000 s(200 frames). The photomultiplier tube(PMT) voltage was maintained at 10. Fluorescence intensity at each time point was quantified using ImageJ software, and the resulting data were analyzed with GraphPad Prism 9.

2.4 CCK-8 Assay

In order to ascertain the biocompatibility of the material in question, 3T3-L1 cells were incubated. Once the cells had reached 80% confluence, the medium was removed and the cells were gently washed three times with PBS. They were then treated with 0.25% trypsin for 1 min. For the purposes of experimentation, 3T3-L1 cells were subjected to centrifugation at 1200 r/min for a period of 3 min. Following this, a suspension of 8000 cells in fresh medium(100 μL) was introduced into each well of a 96-well plate. After overnight incubation, the medium was exchanged for fresh medium containing graded concentrations of TPA-2F or TPA-H(1, 10, 20, 50, 100, 150 and 200 μmol/L), and the cells were cultured for a further 24 h. Subsequently, the medium of each well was removed and replaced with 100 μL of fresh medium containing 10% of the CCK-8 solution (Aoqing Biotechnology, AQ308) for 1 h at 37 ℃. The absorbance at 450 nm was then measured using a microplate reader(Thermo Scientific). The OD values were subsequently used to evaluate cell viability with GraphPad Prism 9 software.

3 Results and Discussion

3.1 Synthesis and Characterization

As shown in Scheme 1, two triphenylamine(TPA)-based derivatives, TPA-H and TPA-2F, were synthesized *via* a Knoevenagel condensation between 4-[bis(4-methoxyphenyl) amino] benzaldehyde and the corresponding 3-(dicyanomethylene) indolin-2-one derivatives, affording yields of 94.1% and 92.5%, respectively. The chemical structures of TPA-H and TPA-2F were fully characterized by ^{1}H NMR spectroscopy(Fig. S1 and Fig. S2, see the Supporting Information of this paper), ^{13}C NMR spectroscopy(Fig. S3 and Fig. S4, see the Supporting Information of this paper), and high-resolution mass spectrometry (HRMS). Furthermore, their molecular structures were unambiguously confirmed by single-crystal X-ray diffraction analysis[Fig.1(A) and (C)].

Single-crystal X-ray diffraction analyses of TPA-H and TPA-2F[Fig.1(A) and (C)] confirm that TPA-H adopts a donor-π-acceptor(D-π-A) architecture, comprising a triphenylamine donor(D), a C=C double bond as the π-bridge, and a 3-(dicyanomethylene)indolin-2-one acceptor(A). Except for the two terminal phenyl rings, the molecular skeleton exhibits a high degree of planarity, which facilitates electron delocalization

over the whole π-system. The pronounced donor-acceptor interaction, extended π-conjugation, and overall structural planarity collectively contribute to the observed red-shift in both absorption and emission[31,32]. TPA-2F shares the same D-π-A framework and shows similar characteristics; moreover, its molecular structure is even more planar than that of TPA-H.

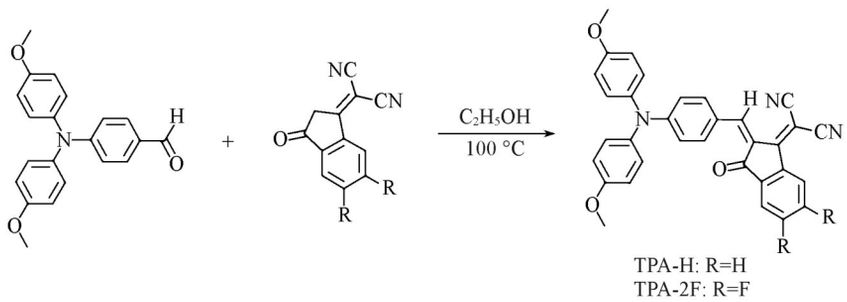

Scheme 1 Synthetic route of TPA-H and TPA-2F

Subsequently, density-functional-theory (DFT) calculations were performed on TPA-H and TPA-2F. Their HOMO orbitals are mainly localized on the triphenylamine group and the methoxy groups, while the LUMO orbitals are largely confined to the planar heterocyclic unit with only a weak contribution from the triphenylamine segment[Fig.1(B) and (D)]. These computational results clearly indicate the occurrence of intramolecular charge transfer in these D-A molecules. Moreover, the band gap of TPA-2F is narrower than that of TPA-H, agreeing well with their absorption spectra mentioned below.

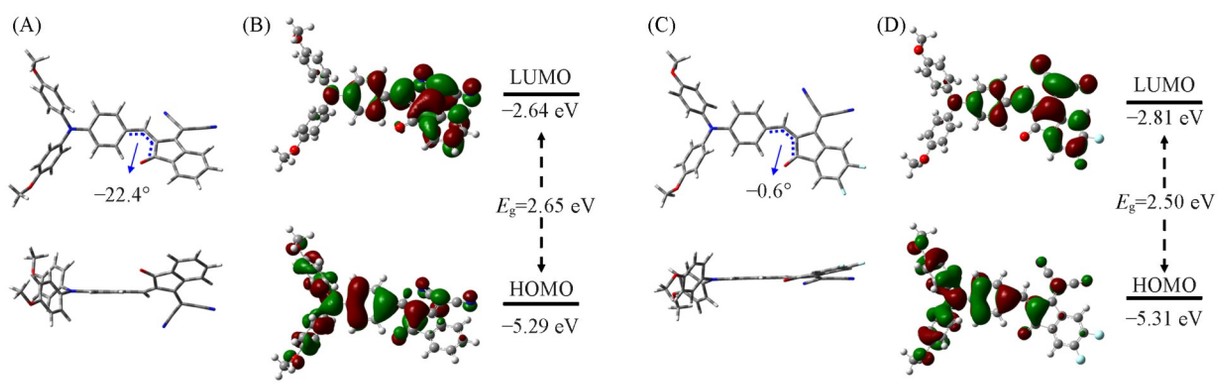

Fig. 1 X-ray crystal structure of TPA-H(A) and TPA-2F(C) and distribution of HOMO and LUMO of TPA-H(B) and TPA-2F(D)

We further investigated the photophysical properties of both compounds. Their absorption maxima in CH_2Cl_2 are located at 574 nm for TPA-H and 586 nm for TPA-2F, respectively[Fig.2(A)]. However, consistent with previous studies[24], the absorption maxima of both TPA-H and TPA-2F also exhibit a slight blue shift with increasing solvent polarity(Fig.S5, see the Supporting Information of this paper).

Both TPA-H and TPA-2F show weak emission in CH_2Cl_2 solution, a phenomenon attributed to the free rotation of C—C single bonds within their molecular structures as previously reported. In contrast, their fluorescence is significantly enhanced upon aggregation. As illustrated in Fig. 2(B) and Fig. S6 (see the Supporting Information of this paper), the fluorescence spectra of TPA-H and TPA-2F were recorded during the gradual addition of hexane to their CH_2Cl_2 solutions. The fluorescence intensity of both compounds rises markedly with increasing hexane fraction, confirming their aggregation-induced emission (AIE) characteristics[33—35]. Consistent with the trend observed in their UV absorption, the emission of TPA-2F is further red-shifted compared to that of TPA-H, likely due to the presence of fluorine atoms, with emission maxima located at 720 and 705 nm for TPA-2F and TPA-H, respectively.

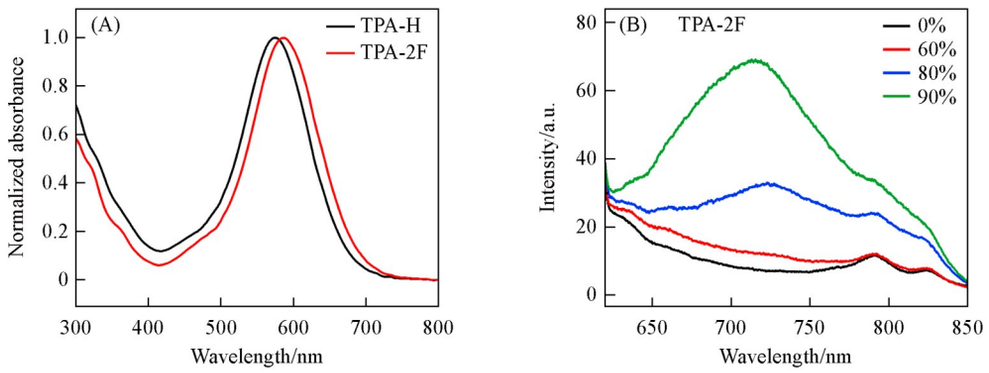

Fig. 2 Normalized absorption spectra of TPA-2F and TPA-H in DCM(A), and fluorescence spectra of TPA-2F as a function of Hex ratio in DCM/Hex mixtures(B)

The excitation wavelength is 580 nm for TPA-2F. The concentration is 10 μmol/L. DCM: CH_2Cl_2; Hex: hexane.

3.2 Performance in Visualizing Early-Stage and Small Lipid Droplets

Prior to biological imaging applications, the cytotoxicity of **TPA**-2F and 2F**TPA**-H was evaluated against 3T3-L1 preadipocytes using the CCK-8 assay. Cells were treated with a range of probe concentrations (1—200 μmol/L) for 24 h. Both compounds showed negligible cytotoxicity at concentrations up to 50 μmol/L, with cell viability remaining above 90%. At 100 μmol/L, viability dropped to approximately 50%[Fig.3(A) and (B)]. This concentration-dependent profile indicates a favorable safety window for imaging applications, confirming the suitability of both probes for subsequent live-cell studies.

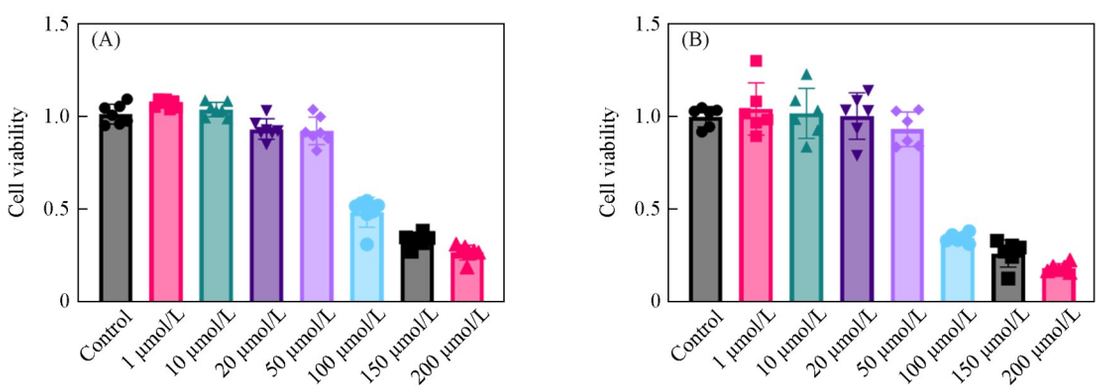

Fig. 3 Cytotoxicity of TPA-2F(A) and TPA-H(B) in 3T3-L1 cells

Cell viability of 3T3-L1 cells after incubation with varying concentrations (1—200 μmol/L) of TPA-2F or TPA-H for 24 h, as determined by CCK-8 assay. Data are presented as mean±SD. Both probes show negligible cytotoxicity at concentrations up to 50 μmol/L, while a significant reduction in cell viability is observed at 100 μmol/L and above.

The subcellular localization of TPA-2F and TPA-H was examined using confocal laser scanning microscopy. Co-staining with commercially available organelle trackers revealed negligible overlap between the signals of both probes and those of LysoTracker Green (lysosomes) or MitoTracker Green (mitochondria), indicating no significant colocalization with these organelles (Fig. S7, see the Supporting Information of this paper). To further assess their targeting specificity toward lipid droplets (LDs), we performed co-staining experiments with the commercial LD dye BODIPY 493/503. As shown in Fig.4, the red fluorescence from TPA-2F or TPA-H overlapped well with the green signal from BODIPY 493/503, confirming their selective accumulation in LDs.

Notably, compared with BODIPY 493/503, both TPA-2F and TPA-H exhibited a superior ability to visualize nascent and small LDs. During live-cell monitoring of LD formation, the TPA-based probes consistently highlighted numerous small, punctate cytoplasmic structures that were only faintly stained by BODIPY (Fig.4). This enhanced performance is likely attributable to the aggregation-induced emission (AIE) character

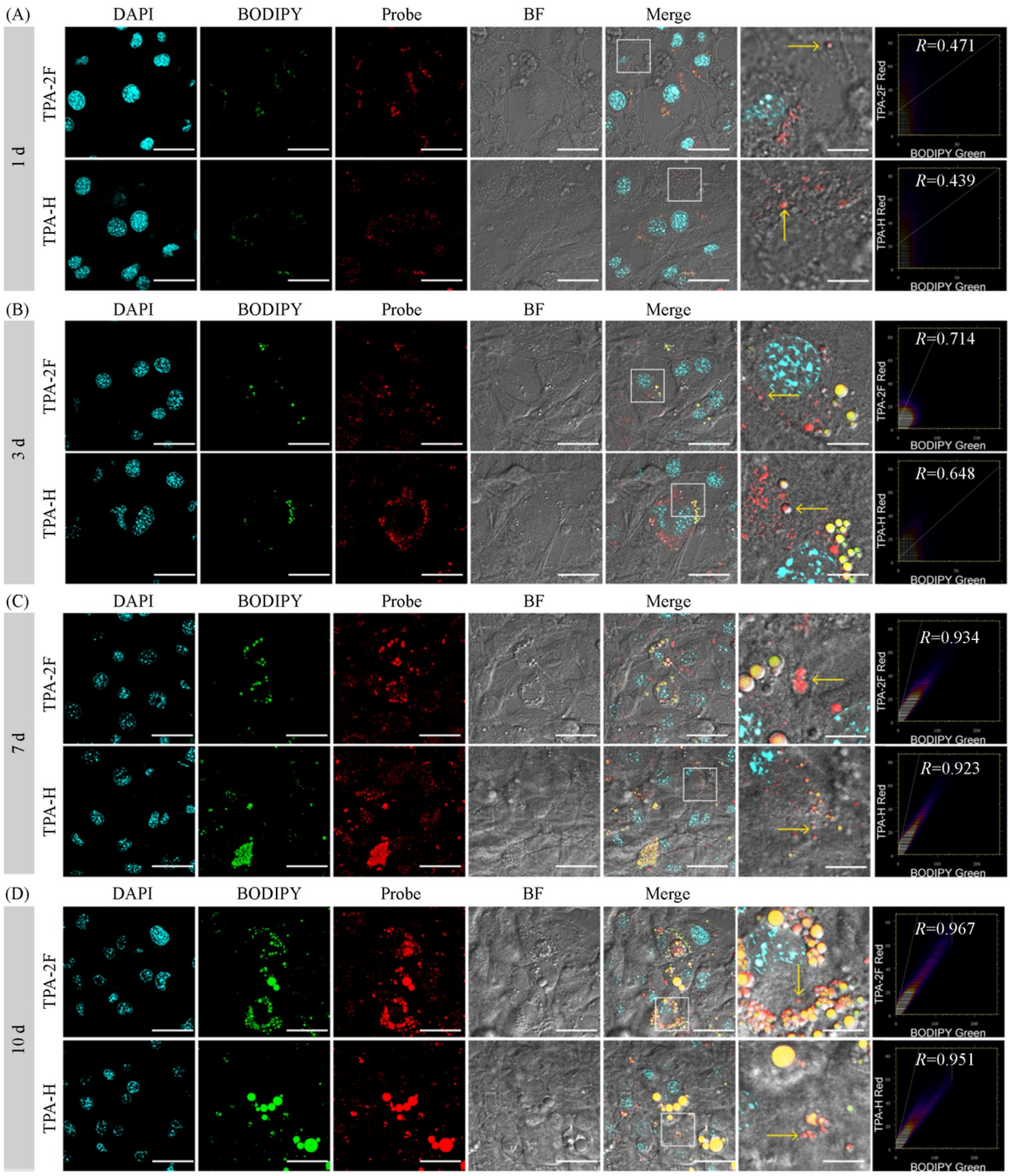

Fig. 4 Dynamic monitoring of lipid droplet formation using TPA-2F and TPA-H

3T3-L1 preadipocytes were induced to differentiate, and cells were stained at day 1(A), 3(B), 7(C), and 10(D) post-induction with DAPI(blue), the corresponding probe(TPA-2F or TPA-H, red), and BODIPY 493/503(green). Bright-field(BF) images are shown in gray. The merged and 4× magnified views(insets) highlight regions of interest. Orange arrows in the magnified images indicate small or nascent lipid droplets that are clearly visualized by TPA-2F or TPA-H but are not readily detected by BODIPY 493/503. The analysis of the Pearson correlation coefficient was performed and plotted using ImageJ. Scale bar: 40 μm, 10 μm(magnified views).

of the TPA scaffold. Unlike conventional dyes such as BODIPY, which often undergo aggregation-caused quenching in the crowded interior of LDs, AIE luminogens (AIEgens) emit strongly upon aggregation. This unique photophysical property allows them to become exceptionally bright within the confined, hydrophobic core of LDs, significantly improving the signal-to-noise ratio and enabling the detection of smaller, lipid-poor

LDs at early stages of biogenesis.

3.3 Photostability of TPA-2F *in vivo*

Photostability is a critical parameter for long-term tracking and super-resolution imaging. The resistance to photobleaching of TPA-2F and TPA-H was evaluated systematically by continuously scanning stained cells under 570 nm excitation. Fluorescence intensity was recorded every 10 s over 200 scanning cycles. In contrast, TPA-H showed a faster decay in fluorescence, undergoing a significant drop after about 50 cycles [Fig.5(A) and (B)]. The superior photostability of TPA-2F is likely attributable to the presence of fluorine atoms, which may shorten the triplet-state lifetime, thereby reducing the probability of reactions with quenching species[30]. This characteristic renders TPA-2F a more reliable probe for prolonged, real-time observation of lipid droplet(LD) dynamics.

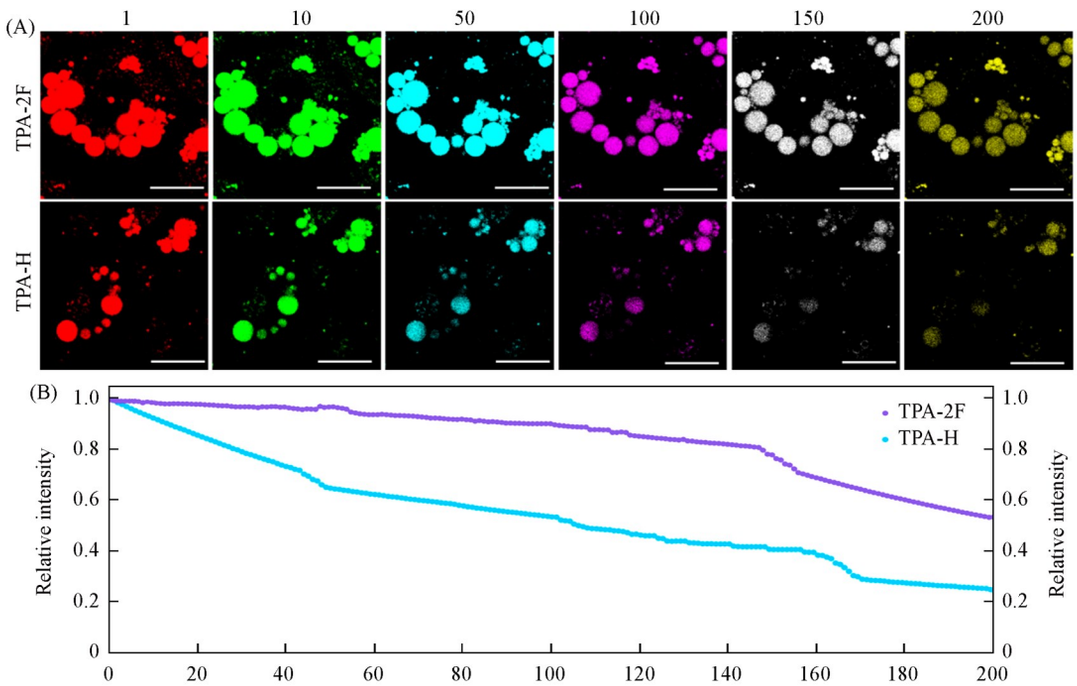

Fig. 5 Photostability comparison of TPA-2F and TPA-H

(A) Representative confocal images of cells stained with TPA-2F(top) or TPA-H(bottom) during continuous laser scanning. Scale bar: 40 μm. (B) Quantitative analysis of fluorescence intensity decay under continuous scanning. Cells stained with each probe were subjected to 200 cycles of laser scanning(570 nm excitation) at 10 s intervals. The relative fluorescence intensity is plotted against the scan number. TPA-2F demonstrates superior photostability, retaining over 90% of its initial fluorescence intensity after 100 scans, whereas the intensity of TPA-H shows a marked decline after about 50 scans.

4 Conclusions

In summary, we have developed two novel AIE-active luminescent probes, TPA-2F and TPA-H, for the specific and high-fidelity imaging of lipid droplets. Both probes display excellent biocompatibility within a practical concentration range and show outstanding targeting specificity toward LDs. Notably, their aggregation-induced emission(AIE) character enables high brightness in the densely packed core of lipid droplets, which allows more sensitive visualization of small and newly formed LDs by comparing with the reported fluorescent probes for LDs(Scheme S1 and Table S1, see the Supporting Information of this paper). Moreover, the strategic introduction of fluorine atoms imparts TPA-2F with exceptional photostability, which significantly surpasses that of TPA-H, rendering it a robust tool for long-term, real-time tracking of LD dynamics. This work not only provides two highly effective probes for lipid droplet imaging, but also underscores the potential

of AIEgens to address the limitations of conventional fluorophores in organelle-specific bioimaging.

The supporting information of this paper see http://www.cjcu.jlu.edu.cn/CN/10.7503/cjcu20200626.

参 考 文 献

[1] Mejhert N., Gabriel K. R., Frendo-Cumbo S., Krahmer N., Song J., Kuruvilla L., Chitraju C., Boland S., Jang D. K., von Grotthuss M., Costanzo M. C., Rydén M., Olzmann J. A., Flannick J., Burtt N. P., Farese R. V., Walther T. C., *Dev. Cell*, **2022**, *57*, 387—397
[2] Liu G., Zheng H., Zhou R., Li H., Dai J., Wei J., Li D., Meng X., Wang C., Lu G., *Biosens. Bioelectron.*, **2023**, *241*, 115707
[3] Mathiowetz A. J., Olzmann J. A., *Nat. Cell Biol.*, **2024**, *26*, 331—345
[4] Scorletti E., Carr R. M., *J. Hepatol.*, **2022**, *76*, 934—945
[5] Ooi G. J., Meikle P. J., Huynh K., Earnest A., Roberts S. K., Kemp W., Parker B. L., Brown W., Burton P., Watt M. J., *J. Hepatol.*, **2021**, *75*, 524—535
[6] Ke J., Pan J., Lin H., Huang S., Zhang J., Wang C., Chang A. C. Y., Gu J., *Adv. Sci.*, **2024**, *11*, e2401676
[7] Cao S., Ding Q., Sun C., Codogno B., Liu Z., Yu X., Kim J. S., Wang K. N., *Angew. Chem. Int. Ed. Engl.*, **2025**, *64*, e202502159
[8] Song Z., Zhang X., Wang Z., Ren T., Long W., Cheng T., Wang Z. L., *ACS Nano*, **2021**, *15*, 18557—18565
[9] Zhou Y., Tian H., Han H., Wang C., Hu X., X. He X., *Chem. J. Chinese Universities*, **2025**, *46*(12), 20250204(周意超, 田贺, 韩海浩, 王辰瀚, 胡习乐, 贺晓鹏, 高等学校化学学报,**2025**, *46*(12), 20250204)
[10] Chen J., Wang C., Liu W., Qiao Q., Qi H., Zhou W., Xu N., Li J., Piao H., Tan D., Liu X., Xu Z. *Angew. Chem. Int. Ed. Engl.*, **2021**, *60*, 25104—25113
[11] Sang M., Huang Y., Wang L., Chen L., Nawsherwan, Li G., Wang Y., Yu X., Dai C., Zheng J., *Adv. Sci.*, **2023**, *10*, e2207066
[12] Guo L., Tian M., Zhang Z., Lu Q., Liu Z., Niu G., Yu X., *J. Am. Chem. Soc.*, **2021**, *143*, 3169—3179
[13] Zadoorian A., Du X., Yang H., *Nat. Rev. Endocrinol.*, **2023**, *19*, 443—459
[14] Farese R. V., Walther T. C., *Annu. Rev. Biochem.*, **2025**, *94*, 447—477
[15] Ramosaj M., Madsen S., Maillard V., Scandella V., Sudria-Lopez D., Yuizumi N., Telley L., Knobloch M., *Nat. Commun.*, **2021**, *12*, 7362
[16] Zhou Y., Hua J., Ding D., Tang Y., *Biomaterials*, **2022**, *286*, 121605
[17] Hsiao W. W., Pham U. K., Le T. N., Lam X. M., Chiang W. H., *Biosens. Bioelectron.*, **2025**, *270*, 116942
[18] Song N., Xiao P., Ke M., Kang M., Zhu W., Huang J., Wang D., Tang B. Z., *Chem. Res. Chinese Universities*, **2021**, *37*, 52—65
[19] Zheng Z., Yang T., Li D., Cao H., Gong J., Liu H., Zhou C., Liu L., Wei P., Gu X., Lu P., Qian J., Tang B. Z., *ACS Nano*, **2023**, *17*, 8782—8795
[20] Lei P., Wei P., Hou L., Dong C., Shuang S., Wang R., *Anal. Chim. Acta*, **2026**, *1384*, 344990
[21] Su H. F., Peng Q. C., Liu Y. U., Xie T., Liu P. P., Cai Y. C., Wen W., Yu Y. H., Li K., Zang S. Q., *Biomaterials*, **2022**, *288*, 121691
[22] Liu H., Yan N., Wong T. Y., Lam H., Lam J. W. Y., Kwok R. T. K., Sun J., Tang B. Z., *ACS Nano*, **2022**, *16*, 14973—14981
[23] Wang J., Kajiwara K., Kesherwani M., Tama F., Ohsaki Y., Yamaguchi S., Taki M., *J. Am. Chem. Soc.*, **2025**, *147*, 41514—41523
[24] Hu Y., Gao X., Ma J., Shangguan Z., Chen L., Zhang G., Zhang X. S., Li C., Li Y., Zhang D., *Aggregate*, **2025**, *6*, e735
[25] Lee M. M. S., Lin D. M., Chau J. H. C., Yu E. Y., Ding D., Kwok R. T. K., Wang D., Tang B. Z., *ACS Nano*, **2023**, *17*, 11039—11053
[26] Gao M., Su H., Li S., Lin Y., Ling X., Qin A., Tang B. Z., *Chem. Commun.*, **2017**, *53*, 921—924
[27] Gao M., Su H., Lin Y., Ling X., Li S., Qin A., Tang B. Z., *Chem. Sci.*, **2017**, *8*, 1763—1768
[28] Pei S., Li H., Chen L., Nie G., Wang H., Liu C., Zhang C., *Anal. Chem.*, **2024**, *96*, 5615—5624
[29] Zheng Z., Yang Y., Wang P., Gou X., Gong J., Wu X., Bao Z., Liu L., Zhang J., Zou H., Zheng L., Tang B. Z., *Adv. Funct. Mater.*, **2023**, *33*, 2303627
[30] Henary E., Casa S., Dost T. L., Sloop J. C., Henary M., *Pharmaceuticals*, **2024**, *17*, 281
[31] Li S., Ling X., Lin Y., Qin A., Gao M., Tang B. Z., *Chem. Sci.*, **2018**, *9*, 5730—5735
[32] Li C., Yao M., Jiang G., Feng L., Wu Y., Sha R., Li Y., Tang B. Z., Wang J., *Angew. Chem. Int. Ed. Engl.*, **2025**, *64*, e202419785
[33] Ding D., Li K., Liu B., Tang B. Z., *Acc. Chem. Res.*, **2013**, *46*, 2441—2453
[34] Shang A., Zhao L., Li Z., Cheng Z., Jin H., Feng Z., Chen Z., Zhang H., Lu P., *Chem. Res. Chinese Universities*, **2022**, *38*, 1461—1466
[35] Chen P., Zhang G., Li J., Ma L., Zhou J., Zhu M., Li S., Wang Z., *Chem. Res. Chinese Universities*, **2024**, *40*, 293—304

(Ed.: F, K)